POLITECNICO DI TORINO
Repository ISTITUZIONALE

Determination of reliable resistance values for electrical double-layer capacitors

(Article begins on next page)

16 July 2022

Determination of reliable resistance values for electrical double-layer capacitors

Lukas Köps [a], Pietro Zaccagnini [b,c], Candido Fabrizio Pirri [b,c], Andrea Balducci [a,*]

[a] *Friedrich-Schiller-University Jena, Institute for Technical Chemistry and Environmental Chemistry and Center for Energy and Environmental Chemistry Jena (CEEC Jena), Philosophenweg 7a, 07743, Jena, Germany*
[b] *Istituto Italiano di Tecnologia, Center for Sustainable Future Technologies, Via Livorno, 60, 10144 Torino, Italy*
[c] *Politecnico di Torino, Dipartimento di Scienza Applicata e Tecnologia (DISAT), Corso Duca Degli Abruzzi, 24, 10129 Torino, Italy*

A B S T R A C T

The power capabilities of supercapacitors are strongly influenced by their passive elements. Within this study, we investigate methods to address resistive components out of galvanostatic measurements and we compared literature methods with the aim to provide a guide to correctly exploit the resistance of supercapacitors. The impact of the sampling conditions of galvanostatic measurements is analyzed and related to electrochemical impedance spectroscopy. Further, a novel method based on the instantaneous power analysis is provided to get real-time information concerning the actual cell resistance during the measurement without altering the galvanostatic experiment. Measurements show that literature methods can provide values close to the series resistance, while the newly proposed power method results in a good estimate of the actual dissipative value.

1. Introduction

Electric double-layer capacitors (EDLCs) can be considered among the most important energy storage devices of our society, and the great interest in these systems is well reflected by their market, which significantly increased in the last 5 years [1]. EDLCs display high power density ($\sim$ 15 kW kg^{-1}) and extraordinary cycling stability and, thanks to these features, they are particularly suited for applications that require fast delivery/uptake of energy. The main drawback of these systems appears to be their limited energy density ($\sim$ 5–8 Wh kg^{-1}), which is significantly lower than that of lithium-ion batteries (LIBs) [2–7]. It has been shown that if the energy of EDLCs could be increased to 15–20 Wh kg^{-1}, the number of applications in which these devices could be conveniently utilized, and could replace LIBs, would increase significantly. For this reason, enormous efforts are currently dedicated towards the realization of high energy EDLCs [8–10]. In the last years, a large number of materials and electrolytes have been developed, and significant improvement have been made possible [11,12]. It is important to remark that in spite the efforts to increase the energy of EDLCs, these devices are, and will remain, high power systems. Consequently, the increase of their energy cannot be made at the expense of a significant reduction of their power.

A fundamental parameter which is affecting any application of EDLCs is the internal resistance (R) [13–15]. EDLCs must be able to handle the high current loads that are used to charge or discharge them within seconds. These high currents are significantly affecting the voltage drop taking place in these devices (due to the Ohm's law) which, in turn, limits their exploitable operative voltage (V). For this reason, in order to avoid a significant loss of performance, the EDLCs manufacturers need to minimize as much as possible R. The equation describing the maximum power (P) of an EDLC , $P = V^2/4R$ is clearly showing the enormous impact of R on the power of EDLCs [16,17].

In spite of the strong influence of R on the cell performance, in literature this parameter is often not adequately considered and only limited information about the resistance of EDLCs are reported. Additionally, there is not a universal or recommended method to calculate R [18–20]. This latter aspect has been addressed in a recent work of Zhao and Burke, in which the authors reported an overview about the different protocols utilized to evaluate the resistance of EDLCs [21]. This lack of information, together with the absence of a widely accepted methodology for the evaluation of R, are making the comparison of the resistance of different EDLCs rather difficult or, in some cases, even not possible.

In this work, we compare different strategies for the determination of the resistance of EDLCs from galvanostatic charge-discharge and

---

impedance spectroscopy measurements. The aim of this study is to supply an indication about the impact of these different strategies on the evaluation of R and to highlight differences between several resistance parameters found for EDLCs. Furthermore, we propose a novel approach to determine the internal resistance of EDLCs from galvanostatic charge-discharge.

2. Material and methods

The evaluation of the resistance reported in the following have been carried out utilizing one lab-scale cell, and two commercial EDLCs.

In the case of the lab-scale cell, the composite electrodes were provided by Skeleton Technologies with a mass loading of 68 g m^{-2} and an electrode area of 1.13 cm^2. In these industrial electrodes, activated carbon is utilized as active material double-sided coated on aluminum foil. One side of the coating was removed to match the experimental setup (see below).

The electrolyte solvent acetonitrile (ACN) was purchased from Sigma-Aldrich with a purity of 99.8%. By the addition of a molecular sieve with a pore size of 3 Å, the initial water content was reduced to below 20 ppm. Tetraethylammonium tetrafluoroborate (TEABF$_4$) was provided by IoLiTec (Germany) and dried before use in a vacuum glass oven at 120 °C and 1×10^{-2} mbar for 24 h. The reported investigation performed with a lab-scale EDLC was carried out utilizing 1 M TEABF$_4$ in ACN with a water content lower than 20 ppm.

The lab-scale electrochemical cell was prepared in a Swagelok-type cell with a two-electrode setup in a Labmaster pro glove box by MBRAUN filled with argon. The content of H$_2$O and O$_2$ of the argon atmosphere was <1 ppm. Two identical electrodes were utilized for the electrochemical cell (symmetrical cell) and separated with a 520 μm Whatman glass fiber disk, soaked with 120 μL of 1 M TEABF$_4$ in ACN electrolyte.

The commercial EDLCs used to carry out the electrochemical measurements for resistance determination were SCMQ14C474PRBA0 by AVX with a rated capacitance of 0.47 F and a rated voltage of 5.0 V as well as B0510-22R5224-R by Eaton with a rated capacitance of 0.22 F and a rated voltage of 2.5 V.

The electrochemical measurements were carried out using a BioLogic VMP-3 potentiostat/galvanostat. Each measurement was repeated for 50 times and the mean values as well as the standard deviations for the galvanostatic charge-discharge measurements were calculated. The galvanostatic measurement of the lab-scale cell was performed with a current rate of 1 A g^{-1} while the commercial cells were cycled with a current based on the total capacitance to end up in a similar timeframe for one charge-discharge cycle. Electrochemical impedance measurements were performed in a frequency range between 500 kHz and 10 mHz and fitted with impedance by applying $R_S - (CPE_{i1} \parallel R_{i1}) - (CPE_{i3} \parallel R_{i2}) - Z_W - C$ as equivalent circuit [22]. R_S was directly obtained from the fitting parameters, while IR was found to be Re(Z) at 10 mHz.

3. Theoretical considerations

3.1. Brief review on impedance spectroscopy definitions

Impedance Spectroscopy (IS) is a powerful method to probe the linear responses of electrical systems in the frequency domain. When applied to electrochemical systems, this technique is addressed to as Electrochemical Impedance Spectroscopy (EIS). Potentiostats mainly implement Frequency Response Analyzers (FRA) to measure impedance ($Z(f)$) or admittance ($Y(f)$) transfer functions by evaluating directly real and imaginary parts of these complex quantities frequency by frequency. The average frequency range of most electrochemical equipment lies within the interval $[1 \times 10^{-6}, 1 \times 10^{6}]$ Hz in which two main processes can be observed: ionic conductivity and electrical double layer (EDL)

formation. Ionic conductivity may comprise eventual charge transfer process and can be observed from medium to high frequencies. EDL formation can be observed from medium to low frequencies and comprises diffusion phenomena of ionic species in (eventually) porous structures.

In the field of EDLCs, EIS can give a clear overview concerning the cell capacitance, which is related to the reactance, and dissipations, which are related to resistances. Literature gives some nomenclature about the real part contributions to the impedance spectra. Some of them are recalled in the following.

According to the impedance spectrum typical for EDLCs displayed in Fig. 1, two main quantities can be identified concerning Re(Z): the equivalent series resistance R_S, also labelled *ESR*, and the electrolyte resistance within the pores or internal resistance Ω. Historically, *ESR* was introduced to describe the non-ideal behavior of dielectric capacitors in which the phase difference was not close to 90°. In this case the phase deviation is due to conduction phenomena in dielectrics. However, this process can be observed at frequencies higher than hundreds of megahertz, hence far from FRA capabilities. Thus, it comes that in systems like electrolytic capacitors and EDLCs, the contributions to the *ESR* value originate mainly from cell characteristics like electrolyte conductivity and parasitic resistances such as ohmic junctions between electrode components. Still, this quantity is computed within IS measurements as Re(Z) when Im(Z) = 0 at high frequencies [23]. In the case of EDLCs, Dsoke et al. showed that some parasitic phenomena concerning intra-particle conduction in non-uniform carbon electrodes can be observed in the middle to high frequency range [14]. Such parasitic phenomena open a semi-circle at the high frequencies whose diameter represents an additive term to the cell resistance. The same phenomenon is well known also in the field of batteries and dye-sensitized solar cells, which contain a current collector with an active material composed by micrometric particles of either of conductive or non-conductive nature [24,25]. Such parasitic contributions and internal resistances should be minimized in EDLC systems in order to guarantee high power
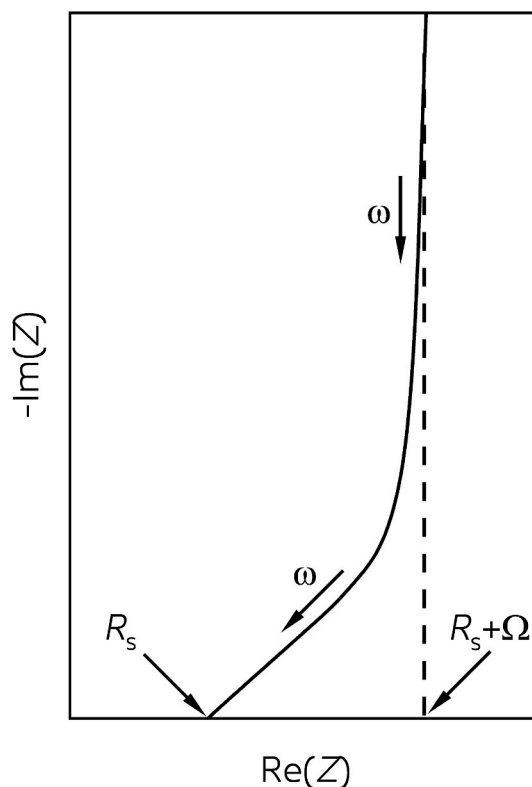

Fig. 1. Generic representation of a Nyquist plot typical for EDLCs with equivalent resistance R_S and internal resistance Ω.

performance. Also, large bulk electrolyte depletion must be avoided in order not to increase the bulk electrolyte resistivity hindering power capabilities.

In some reports, the quantity $R_S + \Omega$ is referred to as equivalent distributed resistance (*EDR*) [26]. This value is obtained by linear extrapolation of the low frequency part of the Nyquist plot, taking the intersection with the real axis. It has to be noticed that when a low slope of the capacitive branch in the diagram is observed, the quantity $R_S + \Omega$ can be underestimated. This is, for example, the case for highly dispersive devices.

According to the Thévenin theory of power sources, the internal resistance of a power generator is given by a series element including all the dissipative elements. In the frequency domain, this definition is still valid, and the resistance value will be the equivalent one shown at fixed frequency. From now on, internal resistance (*IR*) will be used to refer to the actual resistance value according to the Thévenin definition [27].

3.2. Lumped element modeling of EDLCs and electrochemical performances

A widely accepted model for EDLC cells is the one depicted in Fig. 2 [28–30]. In the linear systems theory, an impedance is a transfer function describing the input-output relationship between current and voltage [31]. From now on, current will be treated as input signal and voltage as response.

Linear systems can be treated in both the time and frequency domains. Certainly, the study of linear systems in the frequency domain has its own advantages, but the underlying assumption in both cases is the linearity of the system response. The link between the two domains is given by the Fourier theory. Regardless of the equivalent circuit representation, an impedance can be always written as $Z(f) = |Z(f)|e^{-i\varphi(f)}$ where $|Z(f)|$ is the modulus function of the complex quantity and $\varphi(f)$ represents the real function describing the phase shift evolution introduced by the cell between the current and voltage signals. FRA are used to obtain indirectly these two information since $\mathrm{Re}(Z)$ and $\mathrm{Im}(Z)$ are measured directly. In the time domain, the current is applied during a galvanostatic experiment while the voltage is measured. The measured quantity is the convolution of the current signal with the device transfer function in time domain.

At this point, we believe it is useful to give a different view on the interpretation of certain quantities while evaluating cell performance in time domain measurements. While carrying out a galvanostatic experiment, currents are alternated between positive and negative values and the voltage sweeps linearly within the stability limits. The current signal results to be constant in the semi-periods of charge and discharge. By looking to the overall evolution of the signals, also a galvanostatic experiment can be therefore seen as the application of a time varying signal, a square wave, whose period T is given by the sum of charging and discharging semi-periods. The voltage response can be further seen, ideally, as a triangular wave having the same period as the current control signal. The two ideal signals are depicted in Fig. 3 by the black lines. This means that the measurement is carried out at a certain
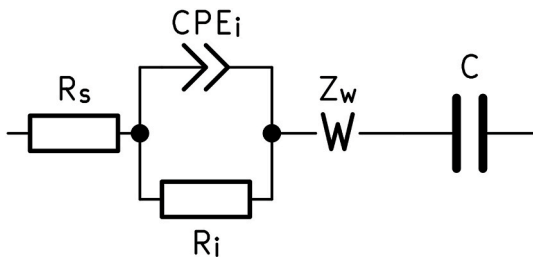

Fig. 2. Simplified model circuit for an EDLC system with R_S representing the equivalent resistance, $CPE_i \parallel R_i$ the electrodes non-ideal behavior, Z_W the Warburg diffusion element and C the cell capacitance.

frequency $1/T$. If this period is in the order of hundreds of seconds, the complete charge discharge cycle has a resulting frequency of tens of millihertz or even less. According to the periodic signal theories of Fourier, both voltage and current signals can be expressed into their spectral components, that is, the infinite sum of harmonics of sinusoidal nature (Fig. 3). Within the approximation of the electrochemical cell behaving linearly in the whole voltage range, one can assume that each of these harmonics at fixed frequency have a linear relationship dictated by $|Z(f)|e^{-i\varphi(f)}$, that is $V(f) = |Z(f)|e^{-i\varphi(f)} I(f)$. The main harmonic, the fundamental one, possesses the same frequency of the wave while the other harmonics are integer multiples of the fundamental: the higher order tones. The amplitudes of these harmonics decrease with increasing tone number.

Hence, while carrying out low frequency time domain experiments, the impedance shows its full dissipative content, which is $R_S + \Omega$ at maximum, i.e., the internal resistance. Consequently, the internal resistance can be directly evaluated from this kind of measurements. In some reports, the quantity evaluated from the voltage drop is claimed to be the *EDR*. From a theoretical and practical point of view, estimating the *ESR* from the voltage drop has several limitations. As it will be shown in the following discussion, the main issues are the determination method and the sampling condition, either to be in time or in voltage. For these reasons, a novel method to evaluate ohmic losses out of time domain experiments, related to the internal resistance, will be considered.

3.3. Power method to evaluate resistive contributions

When dealing with sinusoidal signals, it can be demonstrated that the period averaged instantaneous power $\overline{P} = p(t)_T = v(t) \, i(t)_T$ (with $v(t)$ and $i(t)$ having a phase difference of φ) has two components: one has a non-zero time average which is related to dissipations caused by resistive elements while the other one has zero time average and it is related to reactive elements such as capacitors and inductors. The first one is defined as active power while the second one is called reactive power. In summary:

$$v(t) = V_0 \cos(\omega t + \varphi)$$

$$i(t) = I_0 \cos(\omega t)$$

$$p(t) = i(t)v(t) = V_0 I_0 \left[\cos(\varphi)\cos^2(\omega t) - \frac{1}{2}\sin(2\omega t)\sin(\varphi) \right] \tag{1}$$

Hence, the information concerning both dissipated and stored energy are enclosed within the measured signals. Further, out of these calculations it follows that

$$\overline{P} = \langle p(t) \rangle_T = \frac{1}{T} \int_t^{t+T} p(t)\mathrm{d}t = V_{\mathrm{rms}} I_{\mathrm{rms}} \cos\varphi = Z_0 I_{\mathrm{rms}}^2 \cos\varphi = Re\{Z_0\} I_{rms}^2 \tag{2}$$

where rms stands for root mean square. Effective quantities can be computed for any signal of impulsive nature, while impulsive means that integration over an infinite period returns a finite number. In other words, rms values can be calculated for non-diverging signals. Such quantities are related to the effective delivered intensity, regardless of the wave nature. Hence, to determine dissipative terms, one can integrate the instantaneous power retrieving the total dissipated energy, which averaged over the signal period returns the average dissipated power. This quantity is related then to the effective delivered current to get a resistive quantity which shall be close to the overall device resistance at the time scale of the experiment. That is:

$$IR \sim \quad \mathrm{Re}\{Z_0\} = \frac{\overline{P}}{I_{\mathrm{rms}}^2} \tag{3}$$
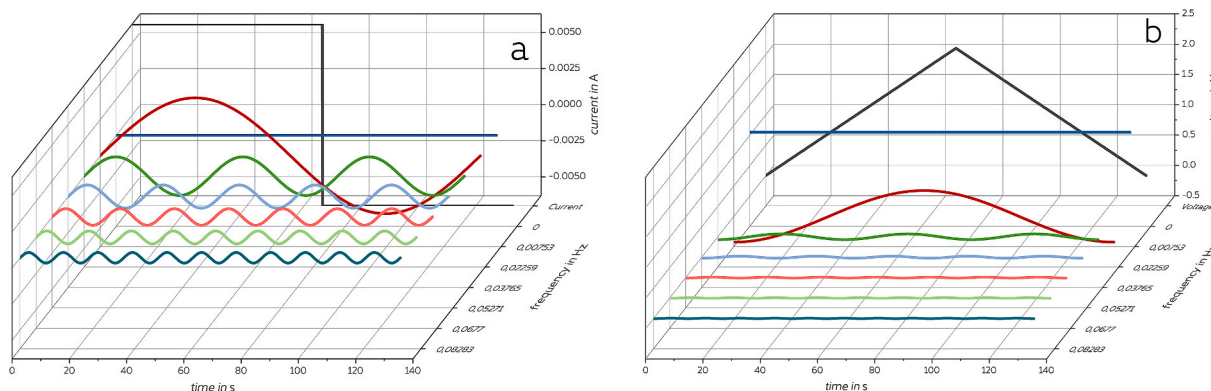
Fig. 3. Transformation of non-sinusoidal, periodic signals of a) current and b) voltage into sinusoidal, periodic signals by fourier analysis.

The approximation symbol was used since the method relies on the strong assumption that the system is behaving linearly. The proposed method returns, in principle, a value related to the low frequency resistance of the electrochemical cell according to the transformation also during aging tests. Such shifts, if there, can be related to changes in values of R_S or Ω singularly or simultaneously due to disparate reasons. The method returns, in principle, a value close to their sum, $R_S + \Omega$, since galvanostatic experiments are carried out at signal frequencies in such a range where the device shows this resistive value.

To summarize, the resistance of supercapacitors can be analyzed utilizing Galvanostatic Charge-Discharge measurements (GCD) as well as Electrochemical Impedance Spectroscopy (EIS) in the frequency domain. Both techniques can be utilized to determine the equivalent series resistance (*ESR* or R_S) as well as the internal or equivalent distributed resistance (*IR* or *EDR*), EIS can be applied to determine precise resistances for comparison of multiple evaluation approaches of GCD data as depicted in Fig. 4 (see Materials and methods).

4. Results and discussion

As mentioned in the introduction, Zhao and Burke recently analyzed and compared the methodologies utilized by different organizations and companies to determine the resistance of EDLCs, pointing out the absence of a standard procedure to analyze this important parameter [21]. In their work, the authors highlighted the use of the IEC test procedure, in which the voltage drop is considered for the determination of the equivalent series resistance (*ESR*) and of the equivalent distributed resistance (*EDR*). In this approach the voltage drop V_{ESR}, needed to calculate the *ESR*, is obtained by the difference between the maximum voltage and value before the curved voltage decrease resulting in linear behavior. On the other hand, the voltage drop V_{EDR}, which is needed for the calculation of *EDR*, corresponds to the difference between maximum voltage and voltage after the curve shaped behavior. The difference between V_{ESR} and V_{EDR} is depicted in Fig. 5. The voltage drop V_{ESR} can be easily determined by the difference between upper voltage limit and the first point of the discharging semi-period. In contrast to this, the voltage drop V_{EDR} equals the difference between the upper voltage limit and the voltage offset at transition time t_0 of a linear regression of the discharging semi-period.

It is important to remark that, due to the non-ideal behavior of the investigated systems and the averaging nature of a linear regression, the calculation of the V_{EDR} might lead to imprecise resistance values. Thus, the selection of the data considered for the linear regression is of extreme importance as it can strongly affect the resulting voltage drop. To face this issue, the IEC test procedure applies the linear regression only for data in the range between 90 and 70% of the maximum voltage [21]. Nonetheless, the possible error in the resulting resistance remains relatively high for the approximation of non-linear behavior.

Taking these points into account, it is evident that the value of resistance calculated for an EDLCs is strongly affected by the method-
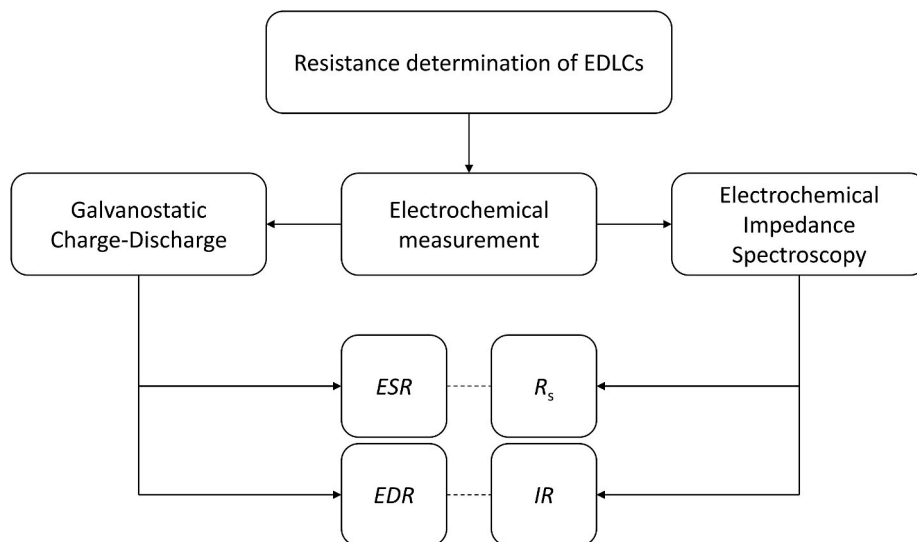

Fig. 4. Summary of multiple evaluation approaches for cell resistances based on galvanostatic charge-discharge (GCD) and electrochemical impedance spectroscopy (EIS).
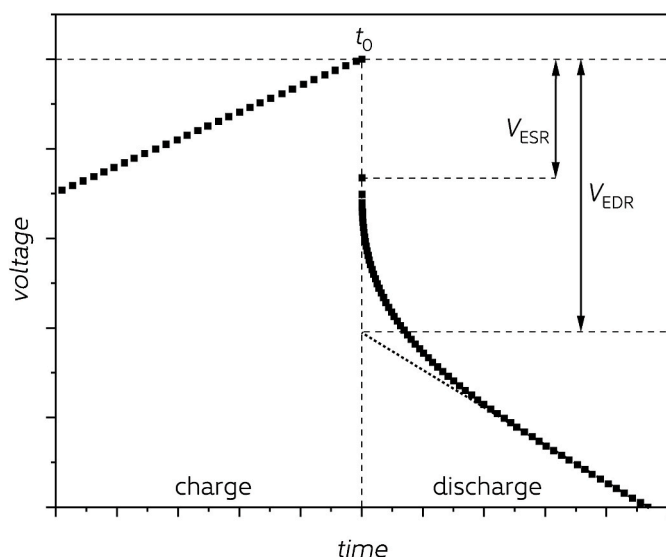
Fig. 5. Schematic representation of the voltage profile of an EDLC focused on the transition from charge to discharge with time at transition t_0 and voltage drops corresponding to *ESR* (V_{ESR}) and *EDR* (V_{EDR}).

ology utilized to calculate this parameter. In order to gain some insight about this important aspect, we therefore considered and compared different methodologies, based on GCD and EIS measurements, which can be used to determine *ESR* and *EDR*. These methodologies were applied to determine the values of these parameters in three different EDLCs: one lab-scale device based on a state-of-the-art electrolyte 1 M TEABF$_4$ in ACN and two commercial EDLCs (Eaton 2.5 V with 0.22 F and AVX 5 V with 0.47 F). All these devices display comparable capacitance.

Typically, the sampling rates of voltage (dV) and time (dt) are playing an important role in GCD measurements since these parameters specify the resolution of the data. In order to understand their impact on the evaluation of the resistance, the variation of one of these two parameters was investigated while setting the other one enormously high to prevent the galvanostat from sampling data due to this condition.

Fig. 6 compares the *ESR* computed from V_{ESR} measured at different sampling rates of voltage dV (a) and time dt (b) by $R = V/2I$ with the resistance R, the voltage drop V and the applied current I. The *ESR* values obtained by the evaluation of GCD data with this specific method are displayed with markers, while R_S values obtained from EIS data are displayed as horizontal lines. Both, different voltage and time sampling rates, show no major effect on the resulting *ESR* since these values remain relatively constant. The values obtained for the standard

deviations of the *ESR* values are in the range of 10 mΩ, and thus cannot be displayed in Fig. 6. Based on this figure, the evaluation of the *ESR* from V_{ESR} seems to constantly overestimate the resistance compared to R_S for all investigated EDLCs. Still, this determination method provides constant values independent on the experimental settings which offers good reproducibility and comparability of *ESR* values.

As recommended by the IEC test procedure, GCD data can be used to calculate the *EDR* by linear extrapolation of the discharge semi-period as shown in Fig. 5. Since an ideal EDLC should show linear discharge behavior in terms of voltage, the range selected for linear regression should not affect the resulting parameters. However, as discussed above, the voltage drop influences the linear regression leading to an underestimated value for V_{EDR}. Thus, the exclusion of points in the beginning of the discharge semi-period would lead to results that are more precise. Fig. 7a shows the *EDR* (markers) obtained by linear extrapolation with different data points considered for the regression. For comparison, R_S (straight horizontal lines) and *IR* (dashed horizontal lines) from respective *EIS* measurements are displayed. For low amounts of excluded points, the computed *EDR* values are significantly underestimating the resistance which should be equal to the *IR* of the EIS measurement. In fact, the values of the Eaton and ACN based EDLCs are closer to R_S while the *EDR* of the AVX cell is in between R_S and *IR*. With increasing amounts of excluded points for linear regression, the investigated EDLCs follow two different trends. While the *EDR* of the Eaton and ACN based EDLCs decreases, the calculated resistance of the AVX device increases due to opposite deviations of the linear discharge behavior, which is shown by the voltage profiles of the discharge depicted in Fig. 7b. The increasing weighting of the latter part in the discharge semi-period amplifies the error further. Since this evaluation methodology could lead to the calculation of negative voltage drops and resistances depending on the discharge curve shape, the resistance determination by linear extrapolation cannot be recommended especially considering the significant difference between the values of *EDR* and IR.

To avoid misleading results due to linear regression and possible deviations based on the voltage profile, a possible approach to determine the voltage drop for *EDR* is to consider a voltage at a certain time after the current change was applied to the EDLC (Fig. 8a). This methodology is less susceptible to the discharge behavior of the cell, but considers the voltage decreased by discharging during this time period as resistance. Fig. 8b depicts the resistances determined from GCD data after different time delays t_{EDR}. As shown, the investigated cells show comparable behavior, displaying resistance values close to R_S for low time delays with increasing resistances at increasing time delays. Considering the short time delay of several milliseconds, it is not surprising that the obtained values are close to R_S, which is computed at t_0.
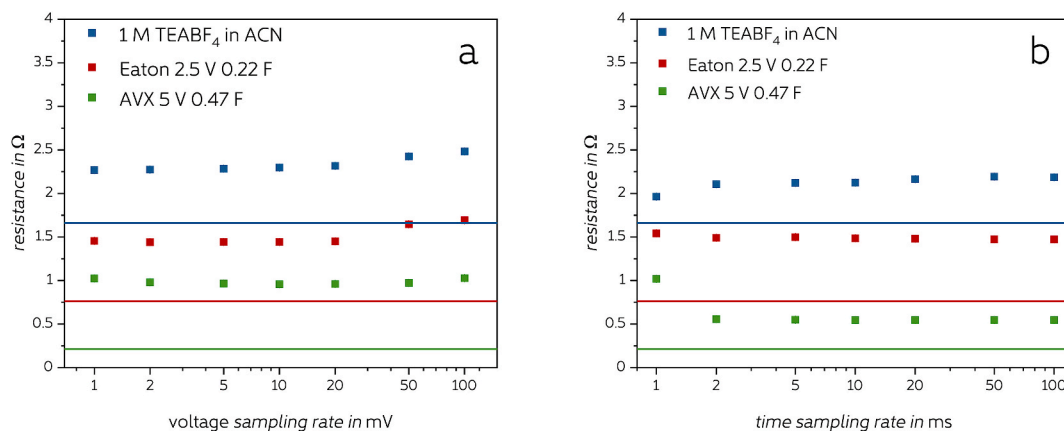

Fig. 6. Comparison of the *ESR* (markers) of a) different voltage sampling rates dV and b) different time sampling rates with R_S obtained from electrochemical impedance spectroscopy (horizontal lines).
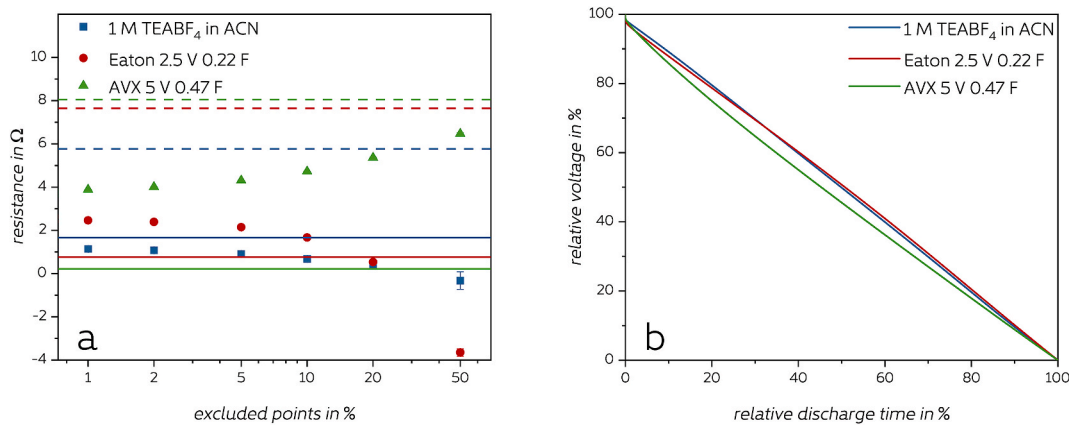
Fig. 7. Comparison of a) the resistance obtained from galvanostatic charge-discharge data by linear extrapolation while excluding different amounts of data points in the beginning of the discharge semi-period from the linear extrapolation (markers) with R_S (straight horizontal lines) and Ω (dashed horizontal lines) obtained from electrochemical impedance spectroscopy and b) the galvanostatic voltage discharge profiles.
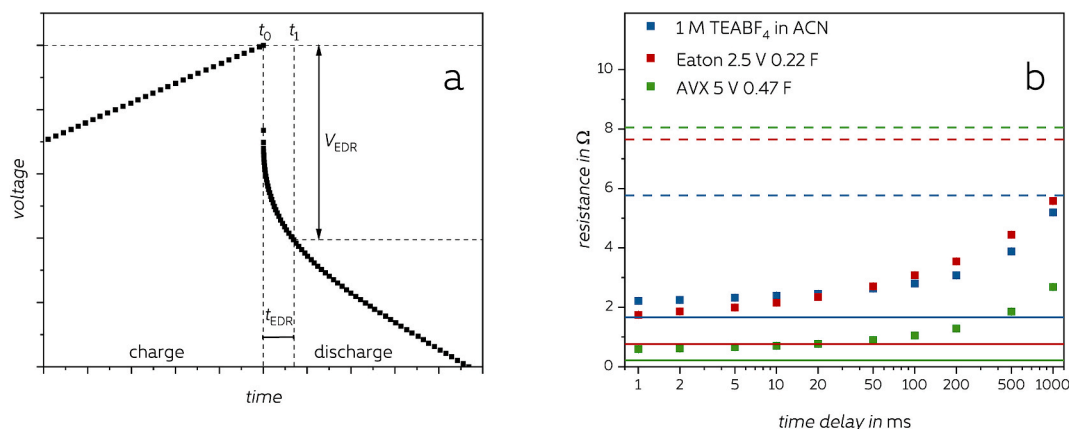

Fig. 8. a) Schematic representation of the voltage profile of an EDLC focused on the transition from charge to discharge with time at transition t_0, time at voltage drop consideration t_1, time delay t_{EDR} and voltage drop corresponding to EDR (V_{EDR}). b) Comparison of the resistance obtained from galvanostatic charge-discharge data by setting different time delays after the beginning of the discharge semi-period to find the voltage drop (markers) with R_S (straight horizontal lines) and IR (dashed horizontal lines) obtained from electrochemical impedance spectroscopy.

Additionally, with increasing time delay, the effect of the discharge comes more into play and increases the resulting resistance. However, this resistance determination methodology provides values which are not similar compared to the IR from EIS but offers a robust way to compute resistances close to R_S independent on the shape of the voltage profile. However, it is important to stress that the chosen time delay should not exceed 100 ms, otherwise the impact of the constantly decreasing voltage becomes too significant.

As described previously in detail, the resistance determination by integrating the instantaneous power shall yield a resistance close to the internal resistance of the device. Fig. 9 depicts the comparison of the resistances obtained by EIS with the resistances based on the power method (IR). The resulting values for the resistance are close to IR for all investigated cells. Additionally, no visible trend around IR is occurring, indicating no systematic over- or underestimating of the total resistance. Considering these results, the power method appears as the only methodology able to offer accurate results for the total resistance obtained from GCD data investigated in this work.

5. Conclusion

In this work, we investigated the influence of different methodologies suitable to determine the resistances of EDLCs from GCD measurements. The comparison with EIS of the respective cells showed that
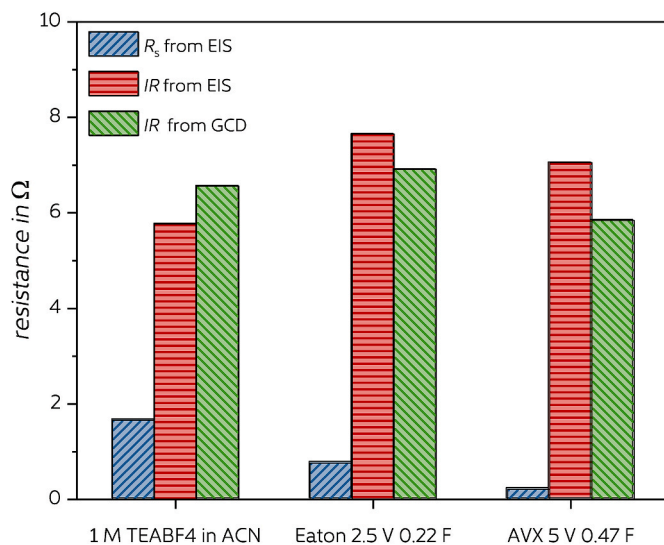

Fig. 9. Comparison of the resistance computed from galvanostatic charge-discharge data by the power method (IR) with R_S and IR obtained from electrochemical impedance spectroscopy.

the determination of the voltage drop based on the difference between the last data point of the charge semi-period and the first data point of the discharge semi-period offers consistent results independent on the settings of the galvanostat. This resulting *ESR* led to values close to R_S obtained by EIS. Surprisingly, resistances from linear regression and time delayed evaluation to obtain values for the voltage drop were not matching the internal resistance *IR* obtained by EIS as expected from literature, but were close to R_S as well. Additionally, we showed that the selection of parameters for the evaluation of the data can significantly affect the results. However, the power method proposed in this work yielded resistance values close to the internal resistance *IR* measured by EIS. This methodology was the only one in this work leading to accurate values for the internal resistance of the EDLC out of GCD data. Furthermore, this novel methodology and accurate ESR extrapolation methods provide a complete cell resistance boundaries determination procedure to be implemented without any galvanostatic test interruption.

Independent on the methodologies covered in this work, it has become clear that the determination of resistances out of GCD data is not a trivial task especially when different resistances should be distinguished. Due to the high number of different approaches in literature, it is difficult to compare results obtained by different groups directly. In the future it will be therefore important to identify a reliable methodology which can be easily applied to commercial and lab scale EDLCs.

Declaration of interest

The authors declare that they have no known competing financial interests or personal relationships that could have appeared to influence the work reported in this paper.

Acknowledgments

References

[1] T.P. Sumangala, M.S. Sreekanth, A. Rahaman, Applications of Supercapacitors, Handbook of Nanocomposite Supercapacitor Materials III, Springer International Publishing2021, pp. 367-393.

[2] F. Beguin, V. Presser, A. Balducci, E. Frackowiak, Carbons and electrolytes for advanced supercapacitors, Adv. Mater. 26 (2014) 2219–2251, https://doi.org/10.1002/adma.201304137.

[3] Z. Lin, E. Goikolea, A. Balducci, K. Naoi, P.L. Taberna, M. Salanne, G. Yushin, P. Simon, Materials for supercapacitors: when Li-ion battery power is not enough, Mater. Today 21 (2018) 419–436, https://doi.org/10.1016/j.mattod.2018.01.035.

[4] Y. Wang, L. Zhang, H. Hou, W. Xu, G. Duan, S. He, K. Liu, S. Jiang, Recent progress in carbon-based materials for supercapacitor electrodes: a review, J. Mater. Sci. 56 (2021) 173–200, https://doi.org/10.1007/s10853-020-05157-6.

[5] J. Zhou, S. Zhang, Y.-N. Zhou, W. Tang, J. Yang, C. Peng, Z. Guo, Biomass-derived carbon materials for high-performance supercapacitors: current status and perspective, Electrochemical Energy Reviews 4 (2021) 219–248, https://doi.org/10.1007/s41918-020-00090-3.

[6] M. Salanne, B. Rotenberg, K. Naoi, K. Kaneko, P.-L. Taberna, C.P. Grey, B. Dunn, P. Simon, Efficient storage mechanisms for building better supercapacitors, Nat. Energy 1 (2016) 16070, https://doi.org/10.1038/nenergy.2016.70.

[7] A. Borenstein, O. Hanna, R. Attias, S. Luski, T. Brousse, D. Aurbach, Carbon-based composite materials for supercapacitor electrodes: a review, J. Mater. Chem. 5 (2017) 12653–12672, https://doi.org/10.1039/c7ta00863e.

[8] C. Schütter, S. Pohlmann, A. Balducci, Industrial requirements of materials for electrical double layer capacitors: impact on current and future applications, Adv. Energy Mater. 9 (2019), 1900334, https://doi.org/10.1002/aenm.201900334.

[9] K.V.G. Raghavendra, R. Vinoth, K. Zeb, C.V.V. Muralee Gopi, S. Sambasivam, M. R. Kummara, I.M. Obaidat, H.J. Kim, An intuitive review of supercapacitors with recent progress and novel device applications, J. Energy Storage 31 (2020), 101652, https://doi.org/10.1016/j.est.2020.101652.

[10] D. Lasrado, S. Ahankari, K.K. Kar, Global trends in supercapacitors, in: K.K. Kar (Ed.), Handbook of Nanocomposite Supercapacitor Materials III, Springer International Publishing, Cham, 2021, pp. 329–365.

[11] P. Simon, Y. Gogotsi, Materials for electrochemical capacitors, Nat. Mater. 7 (2008) 845–854, https://doi.org/10.1038/nmat2297.

[12] A. Balducci, Electrolytes for high voltage electrochemical double layer capacitors: a perspective article, J. Power Sources 326 (2016) 534–540, https://doi.org/10.1016/j.jpowsour.2016.05.029.

[13] K.-B. Li, D.-W. Shi, Z.-Y. Cai, G.-L. Zhang, Q.-A. Huang, D. Liu, C.-P. Yang, Studies on the equivalent serial resistance of carbon supercapacitor, Electrochim. Acta 174 (2015) 596–600, https://doi.org/10.1016/j.electacta.2015.06.008.

[14] S. Dsoke, X. Tian, C. Täubert, S. Schlüter, M. Wohlfahrt-Mehrens, Strategies to reduce the resistance sources on electrochemical double layer capacitor electrodes, J. Power Sources 238 (2013) 422–429, https://doi.org/10.1016/j.jpowsour.2013.04.031.

[15] H. Zhang, Q. Huang, H. Wang, X. Shi, Efficient method to investigate the equivalent series resistance of a capacitor in low frequency range, IET Sci. Meas. Technol. 14 (2020) 494–498, https://doi.org/10.1049/iet-smt.2019.0131.

[16] P. Simon, Y. Gogotsi, Capacitive energy storage in nanostructured carbon–electrolyte systems, Acc. Chem. Res. 46 (2013) 1094–1103, https://doi.org/10.1021/ar200306b.

[17] S. Zhang, N. Pan, Supercapacitors performance evaluation, Adv. Energy Mater. 5 (2015), 1401401, https://doi.org/10.1002/aenm.201401401.

[18] R. Vicentini, L.M. Da Silva, E.P. Cecilio Junior, T.A. Alves, W.G. Nunes, H. Zanin, How to measure and calculate equivalent series resistance of electric double-layer capacitors, Molecules 24 (2019) 1452, https://doi.org/10.3390/molecules24081452.

[19] P.L. Taberna, P. Simon, J.F. Fauvarque, Electrochemical characteristics and impedance spectroscopy studies of carbon-carbon supercapacitors, J. Electrochem. Soc. 150 (2003) A292, https://doi.org/10.1149/1.1543948.

[20] S. Yoon, C.W. Lee, S.M. Oh, Characterization of equivalent series resistance of electric double-layer capacitor electrodes using transient analysis, J. Power Sources 195 (2010) 4391–4399, https://doi.org/10.1016/j.jpowsour.2010.01.086.

[21] J. Zhao, A.F. Burke, Review on supercapacitors: Technologies and performance evaluation, J. Energy Chem. 59 (2021) 276–291, https://doi.org/10.1016/j.jechem.2020.11.013.

[22] M. Murbach, B. Gerwe, N. Dawson-Elli, L.-K. Tsui, impedance.py: a Python package for electrochemical impedance analysis, Journal of Open Source Software 5 (2020) 2349, https://doi.org/10.21105/joss.02349.

[23] B.E. Conway, Electrochemical capacitors based on pseudocapacitance, in: B. E. Conway (Ed.), Electrochemical Supercapacitors: Scientific Fundamentals and Technological Applications, Springer US, Boston, 1999, pp. 221–257.

[24] H.-L. Pan, Y.-S. Hu, H. Li, L.-Q. Chen, Significant effect of electron transfer between current collector and active material on high rate performance of Li 4 Ti 5 O 12, Chin. Phys. B 20 (2011), 118202, https://doi.org/10.1088/1674-1056/20/11/118202.

[25] A. Sacco, Electrochemical impedance spectroscopy: fundamentals and application in dye-sensitized solar cells, Renew. Sustain. Energy Rev. 79 (2017) 814–829, https://doi.org/10.1016/j.rser.2017.05.159.

[26] R. Kötz, M. Carlen, Principles and applications of electrochemical capacitors, Electrochim. Acta 45 (2000) 2483–2498, https://doi.org/10.1016/s0013-4686(00)00354-6.

[27] J.E. Brittain, Thevenin's theorem, IEEE Spectrum 27 (1990) 42, https://doi.org/10.1109/6.48845.

[28] S. Fletcher, V.J. Black, I. Kirkpatrick, A universal equivalent circuit for carbon-based supercapacitors, J. Solid State Electrochem. 18 (2014) 1377–1387, https://doi.org/10.1007/s10008-013-2328-4.

[29] B.E. Conway, W.G. Pell, Power limitations of supercapacitor operation associated with resistance and capacitance distribution in porous electrode devices, J. Power Sources 105 (2002) 169–181, https://doi.org/10.1016/s0378-7753(01)00936-3.

[30] R. Drummond, G. Valmorbida, S.R. Duncan, Equivalent circuits for electrochemical supercapacitor models, IFAC-PapersOnLine 50 (2017) 2671–2676, https://doi.org/10.1016/j.ifacol.2017.08.551.

[31] M.C.H. McKubre, D.D. Macdonald, B. Sayers, J.R. Macdonald, Measuring techniques and data analysis, in: J.R. Macdonald, E. Barsoukov (Eds.), Impedance Spectroscopy: Theory, Experiment, and Applications, John Wiley & Sons, New Jersey, 2018, pp. 107–174.